ISSN 1063-7710, Acoustical Physics, 2010, Vol. 56, No. 6, pp. 794–806. © Pleiades Publishing, Ltd., 2010.

Acoustic Spectroscopy of Fluid Saturation Effects in Carbonate Rock

V. S. Averbakh, V. V. Bredikhin, A. V. Lebedev, and S. A. Manakov

Institute of Applied Physics, Russian Academy of Sciences, ul. Ulyanova 46, Nizhni Novgorod, 603950 Russia

e-mail: swan@hydro.appl.sci-nnov.ru

Received February 20, 2010

Abstract—The results of acoustic spectroscopy of a carbonate sedimentary rock in the case of saturation degree variations are given. The data on the elasticity and dissipation tensors within a two-octave range are obtained for one and the same sample using one and the same measurement technique. High accuracy of the measurements allowed distinguishing all three saturation stages, namely, condensation, meniscus creation, and pore filling with a fluid. The observed variations are in good agreement with the results of a standard granulometric analysis. The character of variations in the frequency dependence of attenuation coefficients make it possible to make reasonable assumption concerning the mechanisms responsible for acoustic energy absorption in porous materials.

DOI: 10.1134/S1063771010060035

1. INTRODUCTION

Resonance acoustic spectroscopy has found wide application as a method for measuring an elasticity tensor of solids and determination of their structural peculiarities [1]. The method is based on a relationship between the spectrum of the sample eigenfrequencies and its mechanical parameters. One of the advantages of this method is the possibility of simultaneously determining both the velocities of longitudinal waves and those of transverse waves within a low-frequency range (unities and tens of kilohertz) in small-size samples. The lengths of test waves used in acoustic spectroscopy substantially exceed the characteristic dimensions of structural inhomogeneities (grains, pores, etc.). Thus, the velocity dispersion attributed to scattering at the structure inhomogeneities exerts no influence [2]. This fact allows comparing the data of field measurements with those obtained under laboratory conditions (e.g., [3]). In addition, the perturbations caused by the converters in the developed setup [4] are negligible.

Note that in spite of the seeming simplicity of implementation, the application of widespread pulsed acoustic methods for the analysis of mechanical characteristics of structurally inhomogeneous porous materials is less preferable for several reasons. First, when pulsed methods are used with an aim to eliminating dispersion attributed to scattering at structural inhomogeneities, the sizes of the analyzed samples should be increased, this complicating control over the experimental conditions. Second, obtaining comprehensive data in case of anisotropic materials necessitates applying multiangle location (e.g., [5, 6]). Third, to eliminate the dispersion attributed to diffraction divergence, it is necessary to increase the radiator aperture and limit the frequency range of probing signals from above [e.g., [7]). Finally, it is necessary to pay special attention to the quality of the converter contact with a sample to obtain absolute values of velocities and elasticity moduli [8]. In addition, use of an adhesive contact of converters can yield partial saturation of a porous sample with the adhesive that substantially changes the properties of the analyzed material [9]. At that, the distribution of the adhesive substantially depends on the unknown pore morphology and, thus, changes in the material cannot be controlled.

Widely used resonance "single mode" methods based on the analysis of the frequencies of the first (simple) modes of longitudinal and torsional oscillations [10, 11] presuppose performing successive measurements first for one type of oscillations and then for the other one. For example, the velocity of the longitudinal waves and corresponding attenuation within a wide frequency range were measured in [11] (see also review [12]) by varying the length of the sample and utilization of higher odd harmonics (below find the comparison of the results of [11] with our data). The velocity of a longitudinal wave and corresponding attenuation were measures on a torsional pendulum where another sample from the same set served as a stiffening element. Thus, it was assumed that the samples cut out from one rock piece are identical. This assumption was checked [11]: the variations in the rod parameters at the specified frequency and in the same external conditions were no greater than 15% in velocity and 6% in attenuation. Thus, it was impossible to measure velocity dispersion.

In addition, it was implicitly assumed that the elements of the measuring system in all sets of measurements and excitation versions exert identical influence on the end result. A distinctive feature of our work was

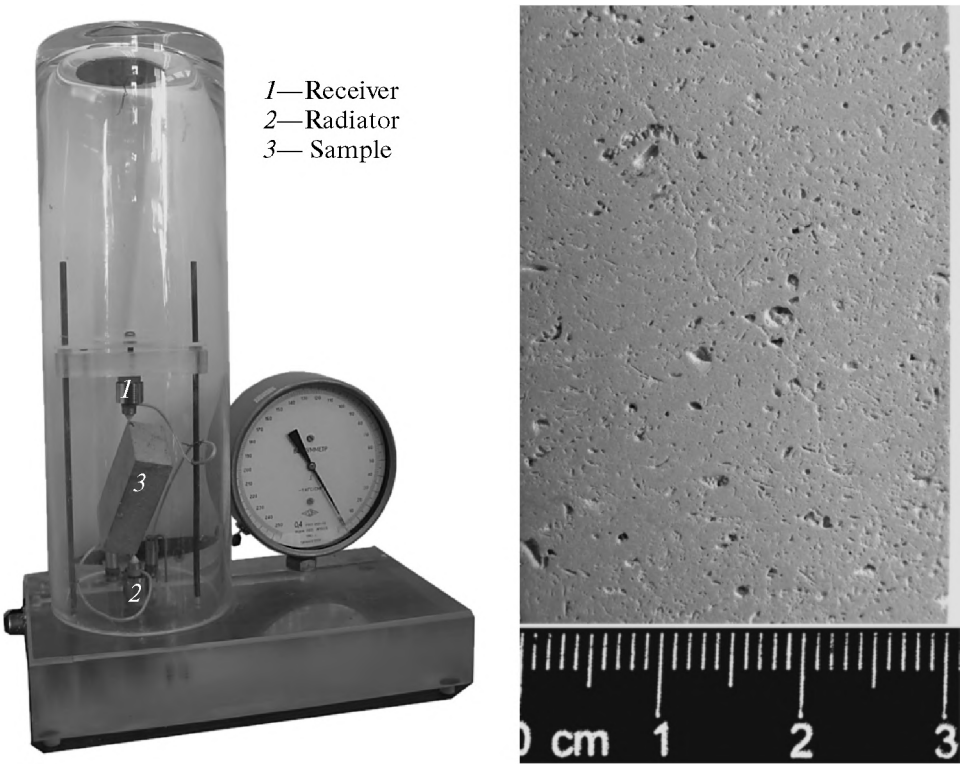

Fig. 1. An experimental setup for measuring acoustic characteristics of consolidated porous materials. The external diameter of the vacuum chamber is 150 mm, the height is 450 mm, and the wall thickness is 10 mm. The characteristic appearance of the surface of the studied material is shown to the right.

simultaneous measurement of the characteristics of longitudinal and transverse waves in one sample within a wide frequency range.

A carbonate rock (dolomitic limestone) was chosen as a specimen to be analyzed based on several considerations. First, carbonates form the main part of silicate rock and about 25% of all sedimentary rock. Carbonates are widely used in industry and construction. Second, many important world deposits of hydrocarbons and sweet water are concentrated in carbonate reservoirs. Third, carbonate rocks are often responsible for development of karst depressions. Fourth, carbonate rocks contain very small grains up to 1 μm in size and are characterized by a developed system of pores that allows hope that interesting dependences of acoustic characteristics on degree of fluid saturation will be found. Finally, the material analyzed in the present study was taken from one of the oldest open-cut mines in Nizhegorod oblast, namely, the Kamenishy mine in the Buturlino region (quarried since the 19th century) and, thus, the obtained data of practical importance.

2. EXPERIMENT

The physical configuration of the experimental setup for measuring acoustic properties is shown in Fig. 1. The geometrical shape of the limestone sample is a rectangular parallelepiped with an angle deviation not greater than 0.1°. The sample dimensions are $98.5 \times 50.5 \times 29.7$ mm^3. The error of dimension measurements is ±0.01 mm. Figure 1 also demonstrates the form of the surface that allows assessment of the sizes of structural inhomogeneities of the material. A visual analysis of the surface using a microscope with a 90× magnification showed that the sizes of hollows and pores vary within a wide range from ~1 to 0.001 mm and even less. The mass of the sample completely saturated with water was $M_s = 366.580$ g; that of a dry sample, $M_d = 339.600$ g. The sample was weighed using a Sartorius LA2000P laboratory balance with an absolute measurement error of ±1 mg at the sample mass less than 1 kg. The density of the sample material was $\rho_s = 2.481$ and $\rho_d = 2.299$ g/cm^3, respectively. These data make it possible to determine the volume of open pores ϕ and the average density of grains ρ_g (the density of the "skeleton" material). Omitting elementary calculations, we obtain that $\phi = 18.3\%$ and $\rho_g = 2.81$ g/cm^3.

The acoustic parameters were measured using the method described in [4, 13, 14]. Oscillations in the sample were excited by a small-amplitude small-pitch tonal signal that ensured a linear mode of oscillations. The oscillations at the measurement instant could be considered as steady-state ones. The velocity variation step was chosen so as to provide for a resolution of

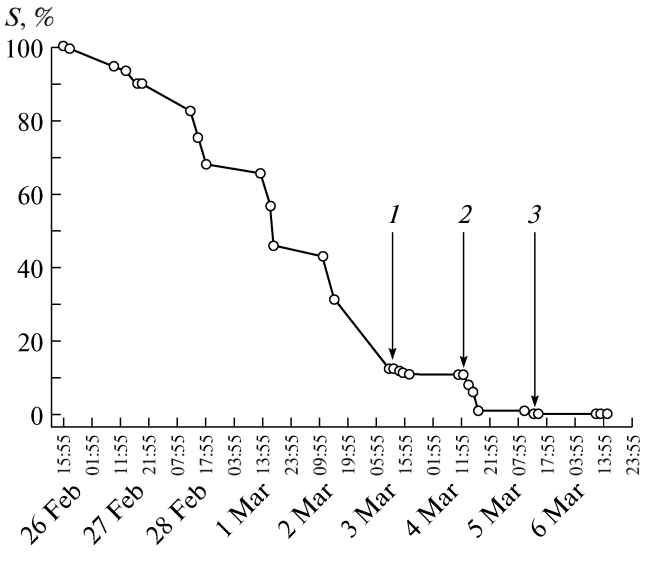

Fig. 2. The character of variations in the degree of sample saturation with distilled water. The data were obtained in 2009.

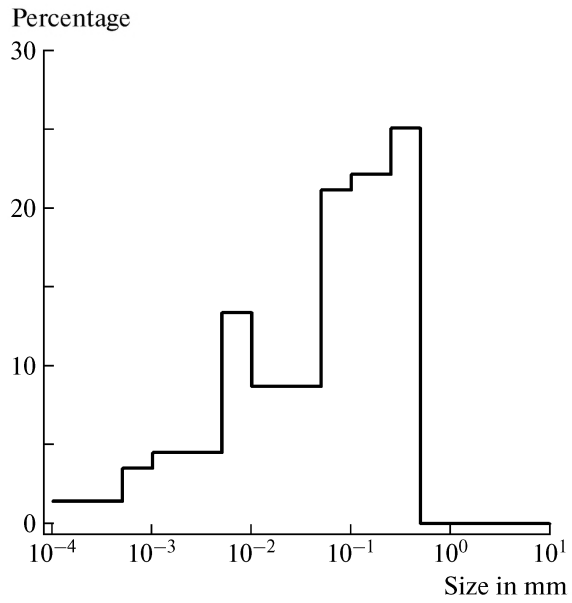

Fig. 3. The histogram of particle size distributions.

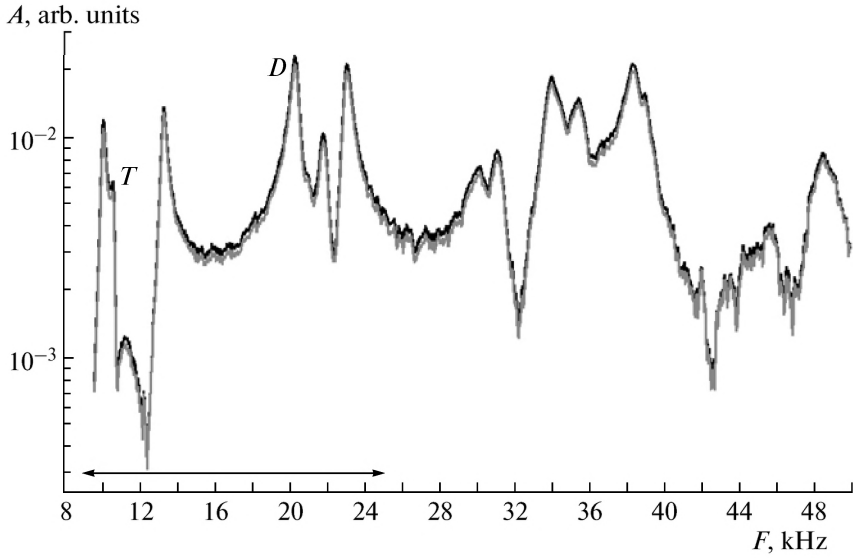

Fig. 4. Reproducibility of the initial data in case of complete saturation. Resonance frequencies of fundamental torsional modes (T) and longitudinal oscillations (D) are marked (see Fig. 5).

overlapping resonant responses [14]. The elasticity moduli of the sample were determined using the method of acoustic spectroscopy [4, 13] as corresponding to the minimal root-mean-square deviation between the measured and the calculated resonant frequencies and the quality of oscillations at corresponding modes.

Macroscopic inhomogeneities are not observed before frequencies of 40 kHz (see discussion of Fig. 6 below). Analysis of the experimental data did not reveal any statistically significant anisotropy of the sample [4, 13] that points to the absence of ordering in the spatial positioning of grains. Thus, the sample can be considered in the analyzed frequency range as a homogeneous isotropic elastic body. The velocities of the longitudinal (V_P) and transverse (V_S) waves were calculated as the ratios $V_P = \sqrt{C_{11}/\rho}$ and $V_S = \sqrt{C_{44}/\rho}$, where standard two-index denominations for the elasticity tensor were used [15].

The degree of saturation was varied as follows. At first the sample was dried in vacuum at the pressure

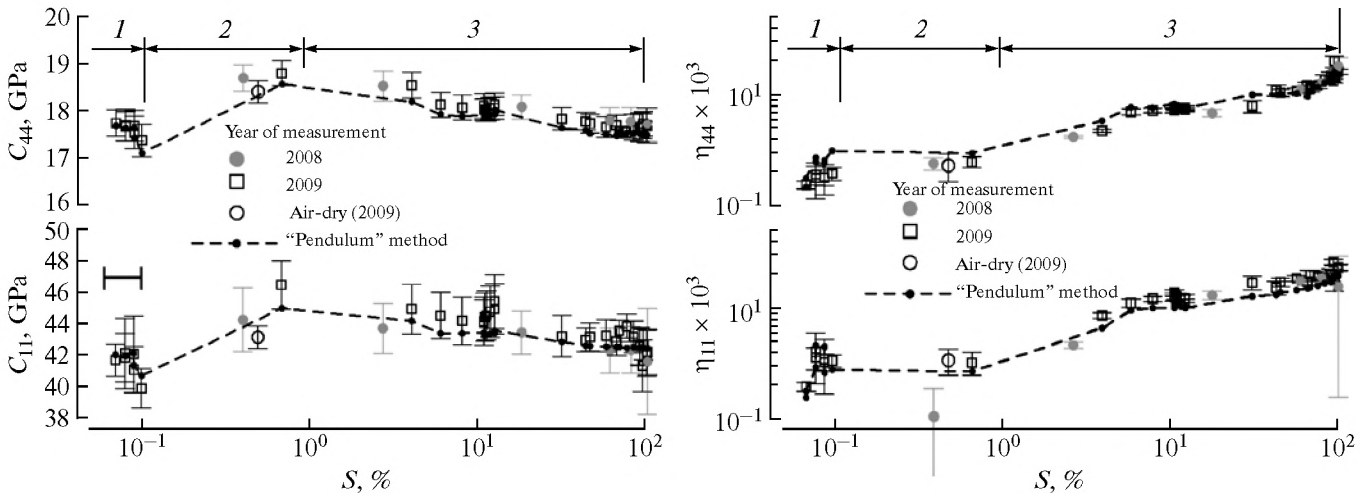

Fig. 5. Elasticity moduli and loss coefficients as functions of the degree of saturation with water. The dependences were constructed using the frequency range marked in Fig. 4. The estimate of the error in determining the saturation degree for the experiment of 2009 ($\Delta S \approx 0.04\%$) is given to the left. The error of the 2006 experiment is $\Delta S \approx 5\%$. Arrows and figures mark characteristic stages of saturation.

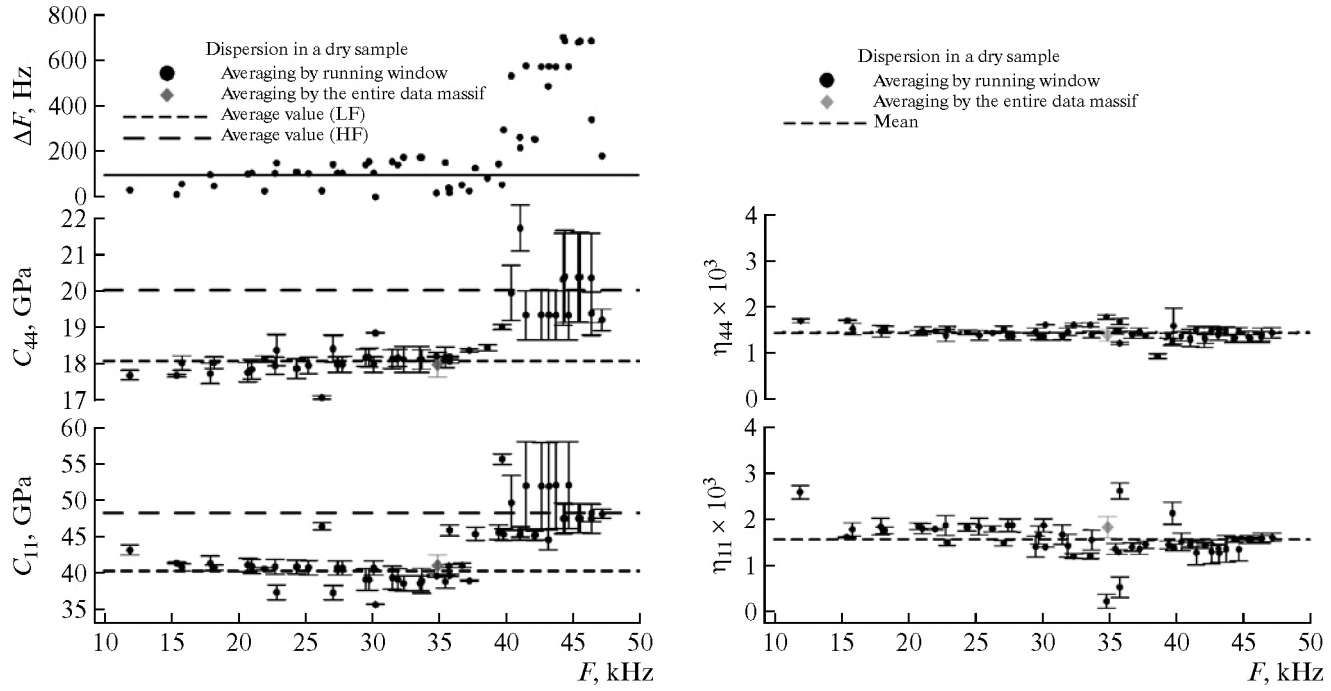

Fig. 6. Absence of dispersion in a dry sample. A solid line in the upper left plot shows root-mean-square deviation between measured and calculated frequencies obtained using the entire body of the experimental data.

which was substantially lower that the pressure of saturated water vapors. Then, again in vacuum, it was saturated with a fluid. For this, a container with distilled water was placed in the same volume (Fig. 1) and the sample was submerged in it. The pressure in the volume was decreased until the fluid began boiling. The excess of gas in the sample pores was released to the vacuum chamber volume, which yielded complete saturation of the pores with the fluid vapors with subsequent condensation. After the gas emission from the sample terminated, the pressure was gradually increased up to the atmospheric one and from this moment acoustic measurements began.

Elementary estimations made based on the Kelvin condensation equation show that when the pressure in the vacuum chamber decreased up to 200 Pa, which is

Table 1. Comparison of the measured values with the estimates obtained based on empirical dependences

	Limestone	Dolomite	Present study
ρ	2.379	2.434	2.481
$V_S^{\dagger}$	1.936	2.666	2.649
$V_P^{\ddagger}$	4.408	4.890	4.277
$V_S^{\ddagger}$	2.345	2.718	2.649

Table 2. Densities and elasticity moduli of the materials forming a base of carbonate rock. The data of [16, 36] were used

	$CaCO_3$	$CaMg(CO_3)_2$	MgO
ρ_g, g/cm^3	2.71	2.87	3.58
K, GPa	73.3	95	162
G, GPa	32	46	131

1/10 of the pressure of saturated vapors at room temperature, the pores with the sizes larger than 0.4 nm are saturated, i.e., all microscopic flaws and hollows inside the sample are hypothetically filled. The degree of saturation was determined by weighing and comparing it with the dry sample mass. A completely saturated sample preserved its weight in a closed volume at room temperature during a long period of time, the time constant being several days. This means that there were constant conditions during each 1-h-long run of acoustic measurements where the analyzed sample was found.

The protocol of variations in the moisture concentration in the sample is shown in Fig. 2. The arrows in the figure show the following instants: (1) beginning of the process of pressure decrease in the vacuum chamber (Fig. 1), (2) a pressure decrease up to the level lower than the pressure of saturated vapors (sample drying), and (3) sample heating in a microwave oven up to 150°C for 3 min with subsequent placing into a vacuum chamber with a silica gel (removal of residue moisture).

It is useful to compare the data of our measurements with the known results obtained earlier by other authors using another measurement technique [16]. The comparison results are listed in Table 1. The values marked with $^{(\dagger)}$ were obtained from the Pikit regression dependences $V_S(V_P)$ (the approximation error was about ±3%) [12]. The values marked with $^{(\ddagger)}$ were obtained from the regression dependences $V_{P,S}(\phi)$. The density corresponds to the regression dependence $\rho(V_P)$. The error of all these empirical dependences is 5–10%.

It can be easily seen that the material parameters of the sample studied in the present work are close to the averaged parameters of limestone and dolomite (in the Kamenishy open pit mine, they extract dolomitic rock for production of crushed rock). On the one hand, it is in good agreement with the data of chemical and mineralogical analysis (see below). On the other hand, it shows that the studied sample does not have any acoustic property anomalies and can be considered as a typical representative of carbonate rocks.

The data listed in Table 1 show that the studied sample consists of limestone (calcium carbonate) and dolomite. Table 2 gives the densities and strengths of these minerals. The last column gives the data for periclase, which is also present in dolomites [16] and, according to the chemical analysis data (see below), is found in the analyzed sample. The density of the "skeleton" or an equivalent sample with zero porosity was $\rho_g = 2.81$ g/cm^3 that corresponds to the ≈2/3 ratio of calcite and dolomite in the sample.

The specialists of the Volga-Geologiya FGUGP Central Laboratory (Nizhni Novgorod) performed analysis of a limestone sample that included (1) petrographic studies, (2) investigations of the mineralogical composition, (3) chemical analysis, and (4) investigations of the granulometric composition.

According to the microsection description, the sample is a high-gray strongly porous limestone dolomite. The inner structure in micrograin and the rock consists of dolomitic grains 0.01–0.02 mm in size that form a micrograin mosaic structure. The grain shape has the form of feebly marked rhombohedrons, which are sometimes round-shaped. The rock is inhomogeneously porous with the sections covering 30–40% of the microsections. The shape of the pores is irregular, sometimes roundish, sometimes elongated. The pores are 0.05–10 mm in size. Based on the results of mineralogical analysis, the sample represents a carbonate rock with inclusions of mica.

The chemical analysis after thermal processing showed that the main components of the sample are as follows: CO_2 41.1%, CaO 31.1%, and MgO 19.4%, which makes up 97% of the sample's volumetric content. Three dominant components are calcite $CaCO_3$, dolomite $CaMg(CO_3)_2$, and periclase MgO in the following proportion: 43.4/42.6/11.1 (in %). The calculated density of the "skeleton" is 2.80 g/cm^3, in good agreement with the measurement data: ρ_g = 2.81 g/cm^3. The chemical analysis revealed the presence of SiO_2 (1.5%), Al_2O_3 (0.3%), Fe_2O_3 (0.2%), and Na_2O (0.1%). These components are elements of micas whose presence was found during the mineralogical analysis. The results of the granulometric composition analysis are shown as histograms in Fig. 3. It can be easily seen that the limestone consists of particles with sizes from 0.1 μm to 0.5 mm.

Let us calculate the elasticity moduli within the framework of the known models of effective media [16, 17]. Table 3 lists the measured and the calculated moduli for C_{11} and C_{44} in GPa. Version (1) corresponds to the composite from spherical particles with different sizes, each consisting of calcite, dolomite, or peri-

clase in the volumetric proportion corresponding to the skeleton density in the absence of hollows. Spherical hollows inside the sample with the porosity corresponding to that measured in the studied sample ($\phi = 18\%$) are taken into account in version (2). Version (3), in addition, takes into account a small number ($\phi_1 = 0.1\%$) of hollows shaped as narrow cracks, their volumetric concentration parameter, which does not depend on the choice of the relative thickness of the crack being $\phi_{crack} = 24\%$. The used models are described in detail in [16, 17], and here we omit details and bulky formulas applied during the calculations.

By comparing the quantities listed in Table 3 we can make a conclusion that the data of acoustic measurements are in good agreement with the data of the chemical analysis and petrographic investigations (grain shape) given above. The necessity to take into account a small volumetric concentration of cracks is in good agreement with the revealed presence of mica the splitting of which yields formation of these extended flaws. Thus, the acoustic data for dry limestone can be satisfactorily explained within the frame work of elementary model considerations.

3. DEPENDENCE OF ELASTICITY MODULI AND LOSS FACTOR ON THE DEGREE OF SATURATION

The analysis of variations in the acoustic properties depending on the saturation degree is interesting from the point of view of both the understanding of the mechanisms of a liquid phase interaction with the skeleton of a porous medium within the frameworks of the known models of Gassman, Bio, Mavko, et al. [16] and from the applied point of view for construction of diagnostic systems intended for the search of reservoirs filled with hydrocarbons or sources of pure water (e.g., [12]). When exploiting natural reservoirs, variations in the elasticity moduli attributed to a physical-chemical interaction of the skeleton and the fluid that fills its pores are capable of affecting the equilibrium state of the rock and can yields nonelastic compression under the action of lithostatic pressure and ground depressions on the surface [18].

When analyzing the effects of saturation with a fluid, it is necessary to thoroughly check reproducibility of the results and stability of the conditions under which the measurements are performed [12]. The data of Fig. 2 point to invariability of the acoustic measurement conditions. Figure 4 shows acoustic responses within a broad frequency band for the first two records corresponding to complete saturation which were obtained with a 1.5-h interval. It can be seen that the responses repeat themselves practically completely not only in the positions of frequencies and maximum amplitudes, but in minor details as well. The data for other saturation values behave themselves analogously. Thus, the conditions of performing acoustic measurements were stationary.

Table 3. Measured and calculated elasticity moduli of a dry limestone sample. The numerator gives the values corresponding to averaging taking into account the volumetric concentration of fractions uniformly distributed in the material with the maximal concentration, namely, the matrix. The values corresponding to the solution of self-consistent problems when all fractions are considered as equipollent are given in the denominator

Elasticity moduli	Measured values	Estimated quantities		
		Version no. 1	Version no. 2	Version no. 3
C_{11}, GPa	41.7 ± 1.0	146.5/133.8	90.8/72.2	46.6/37.1
C_{44}, GPa	17.8 ± 0.3	43.3/38.2	28.8/24.6	20.4/18.6

The arrows in Fig. 4 show the frequency range where seven lowest modes are well excited and are seen on all records at ant values of saturation with a fluid. This very frequency range was used for constructing the dependences given in Fig. 5. In the range of frequencies higher than 25 kHz in the case of a practically complete saturation the mode resolution was difficult owing to a high signal-to-noise ratio (see the data of Fig. 4).

The dependence of the elasticity moduli C_{ij} and the loss factors η_{ij} on the degree of saturation is demonstrated in Fig. 5. Here and hereinafter, we mean that the loss factor η_{ij} is a quantity that is inverse to the quality of oscillations of a corresponding type. Attenuation at the distance equal to the wavelength is related to the loss factor by an elementary relation: $\exp(-\pi\eta_{ij})$. One plot gives the results of the experiment of 2009 performed at the controlled measurement conditions and than of 2006 when saturation was constantly varied during the measurements owing to evaporation of water to the room volume. In this case, the saturation was calculated based on the results of calibration measurements of the time dependence of resonance frequencies and quality on the mass of the fluid inside the sample and a sample mass decrease.

It can be easily seen that the dependences obtained in 2006 are qualitatively reproduced in the experiment of 2009 and the accuracy of 2009 experiments is substantially higher. The saturation parameter for a dry sample $S = 0$ was deliberately changed to $S \approx 0.1\%$ and the experimental points were separated with an aim to show the tendency of acoustic parameter variations in case the saturation for a nearly dry sample changed. A blank circle shows the results of the measurements for an air-dry sample performed 2 weeks after the main run of experiments. It can be seen that after heating and drying there were no irreversible changes in the sample characteristics.

In Fig. 5 we also give the dependences of the moduli C_{11} and C_{44} as well as losses η_{11} and η_{44} obtained using the method used in [11]. This method can be called a "pendulum" method or the method of a reso-

nant rod since in this case only lower forms of longitudinal and torsional oscillations (marked in Fig. 4) are analyzed. The errors in C_{11}, C_{44}, η_{11}, and η_{44} depend on the accuracy of measuring corresponding frequencies and qualities. The frequencies and qualities were measured using the method of matched filtering [14], which provided for determination of corresponding quantities with an error of 0.1–0.5%. By comparing the data shown in Fig. 5, we can see distinctions of kind between the measurements performed using the method of a resonant rod [11] and those obtained using the method of acoustic spectroscopy.

When the method of acoustic spectroscopy is applied the data corresponding to all modes of the sample oscillation in the analyzed frequency range are "weighed." The errors attributed to both the error in measuring frequencies and qualities and the error of the effective solid model itself [1] decrease. When the "pendulum" method is applied, there is one measurement for each sought parameter. Thus, the errors are not averaged. Though the dashed lines in Fig. 5 qualitatively repeat the data corresponding to the measurements performed using the method of acoustic spectroscopy and both results coincide with the confidence interval accuracy the estimation of the parameters in the "pendulum" method has an unknown systematic error.

When carefully reading [11] one can notice that the author points to systematic deviations in the data on the velocities of elastic waves equal to ~12–15% for different samples. These systematic deviations should be treated as an error of initial model considerations. The data obtained by us turned out to be much more accurate [11]. The average error of elasticity modulus measurements is $\delta C_{11} = 3.6\%$ and $\delta C_{44} = 1.9\%$ that corresponds to the error of elastic wave velocity measurements $\delta V_P = 1.8\%$ and $\delta V_S = 0.9\%$ and is nearly one order higher [11]. The average error of measuring the loss factor, namely $\delta\eta_{11} = 12\%$ and $\delta\eta_{44} = 8.9\%$, is nearly the same in our measurements as that in [11].

The resonance frequencies were measured within the range of 10.6–49.4 kHz that allowed performing the analysis of frequency dependences of both the elasticity moduli and the losses during variations in the degree of saturation. Note once again that contrary to [11] all measurements were performed using one and the same sample. The frequency dependence was analyzed using the technique described in [13]. The elasticity tensor and the dissipation tensor were estimated using a running window with overlapping that made it possible to obtain a representative plot of the frequency dependence for both tensors.

Figure 6 shows frequency dependences $C_{11}(f)$, $C_{44}(f)$, $\eta_{11}(f)$, and $\eta_{44}(f)$ for dry limestone. The dependences shown in Fig. 6 were plotted using the windows of averaging by three, five, seven and ten frequencies, which yield practically similar estimates of the quantities of interest. An increase in the elasticity moduli in the range of high frequencies with a simultaneous increase in the model error (the upper curves on the plots) points to the effect of a macroscopic inhomogeneity. This inhomogeneity was seen with the naked eye as a dark region on the sample surface and occupied nearly 1/8 of its volume. Individual spikes on the plots (Fig. 6) are related to a small number of averaging (three frequencies in the averaging window). The expected dispersion of the elasticity moduli corresponding to the measured loss factor values is 0.13%, which is beyond the reached measurement accuracy.

Figure 7 plots frequency dependences of the loss factor η_{44} with the minimal measurement error at different degrees of pore filling with a fluid. the data for the frequencies higher than 40 kHz are omitted since, as is apparent from Fig. 6, the effect of the macroscopic inhomogeneity inside the sample is substantial in this region. The data of Fig. 7 allow asserting that the absorption maxima in the considered frequency range are absent. Dispersion of the elasticity moduli was not revealed either (the data are not given). The frequency dependence pf the loss factors is discussed in Section 4.3.

4. DISCUSSION OF THE RESULTS

It is interesting to compare the results we obtained with the known literature data (see [12, 18]). Initially, Gassman and then Bio in their models assumed the shear modulus during filling of pores with a fluid to be constant (see [16]). A decrease in the shear wave velocity during pore saturation with a fluid was related to an increase in the integral density of the porous material. Later, a deviation from the initial assumptions of the Gassman–Bio models that manifested itself as a change of the shear modulus during pore filling with a fluid was revealed. The revealed variations turned out to be substantial and depended on the type of the fluid filling the pores. It is important to note that the observed effects were not related to dissolving of the parent material in a fluid and are reversible.

The effect of a fluid on the shear modulus should be considered in a greater detail. More often, as in Fig. 5, the shear modulus decreases with saturation of pores with a fluid. Polar fluids (e.g., water) yield the maximum variations in the shear modulus. An increase in the elasticity moduli during saturation of the rock containing clay particles with a fluid was also observed. It was related to clay swelling and improvement of cohesion between the grains.

One more mechanism has a physical-chemical nature and is closely connected with strength characteristics, namely, cohesion forces, as it was shown in the experiment performed by Obreimov with mica in the 1930s. A monomolecular fluid layer decreases the surface energy and the cohesion forces owing to a decrease in the surface tension coefficient at the solid–fluid interface as compared to that at the solid–

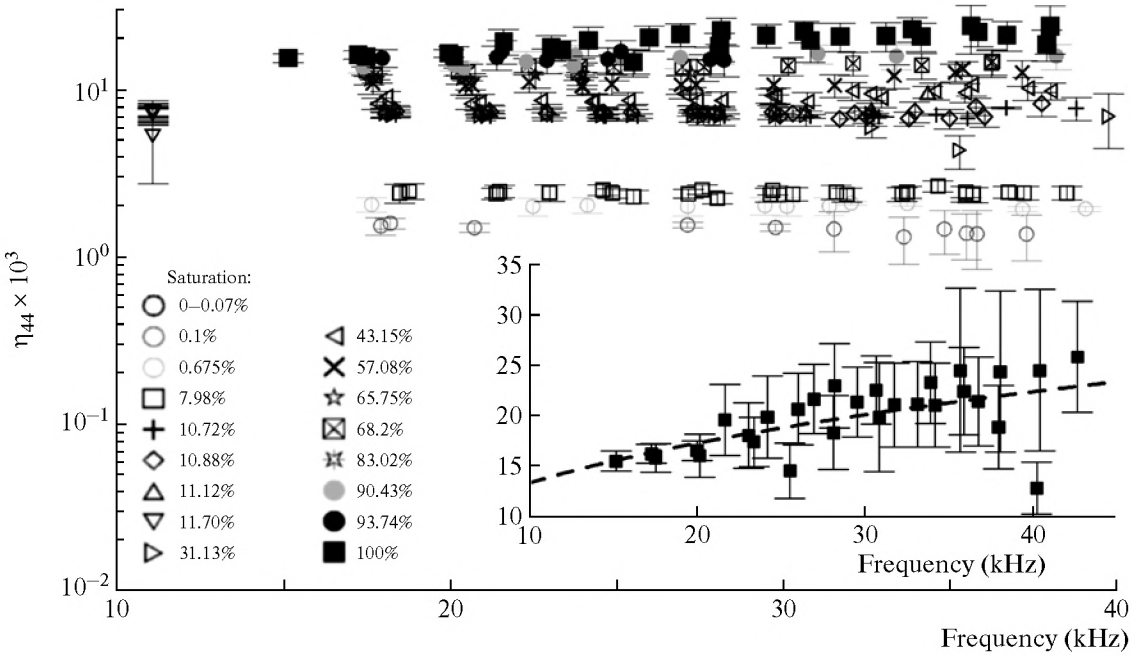

Fig. 7. Frequency dependences of loss coefficients as functions of the degree of pore saturation with a fluid. The data for η_{44} in case of complete saturation are given in the insert.

gas interface (see [12]). In addition, a fluid and, in particular, a polar fluid decreases the Gamaker constant, which determines the intensity of the Van der Waals forces acting at a microscopic level of contacts of individual grains, which yields corresponding variations in macroscopic acoustic characteristics [19]. One more mechanism of the influence of a small amount of water on the elasticity moduli of silica-containing materials is associated with the formation of monomolecular layers of water, beginning of chemical processes, and formation of silica gel polymer chains, which additionally bond the grains [20] and create compression pressure. This mechanism is rather related to unconsolidated media which were considered in [20]. In this case, cementing substances which bond the grains are initially absent and a fluid yields formations of such bonds and, as a result, noticeable variations in acoustic properties.

Thus, the analysis of the literary data shows that it is difficult to distinguish one mechanism responsible for variations in elasticity moduli and, in particular, the shear modulus. Thoroughly performed experiments [18] reveal a high correlation between relative variations in the shear modulus and the area of the free surface of pores.

Let us compare the obtained data with the results of [11], which are often considered in the literature as reference ones (see [12, 16]). Such a comparison is justified since the average size of grains and porosity of the materials considered by us (see above) and in [11] are close. The dependence of losses on the degree of saturation measured by us qualitatively agrees with that obtained in [11]. Our results, as well as the results of other authors (see review [12]), show that addition of water vapors and subsequent water condensation on the grain contacts yields a substantial increase of losses during propagation of elastic waves in porous bodies. Further saturation with a fluid results in a monotonous growth of elastic wave attenuation. However, there are some quantitative differences. In [11] the attenuation doubles, and the data of Fig. 5 correspond to a 20-fold increase of losses that point to a larger contribution of a fluid into dissipative processes in carbonate rock as compared to sandstone considered in [11].

The authors of [11] marked a nearly twofold increase in velocities of longitudinal and transverse waves (and a fourfold increase in the elasticity moduli) with a decrease of the degree of saturation below 2%. Our data reveal 10% relative variations in the elasticity moduli within the entire range of saturation changes (S = 0–100%). The obtained character of elasticity moduli variations, depending on the degree of saturation, qualitatively differs from the results of [11] which are reproduced in many works (e.g., [12, 18, 21]). Figure 5 shows characteristic stages of saturation with a fluid, and we can clearly see an S-shaped form of the dependences on elasticity moduli on the degree of saturation with a fluid. The existence of the minimum of C_{11} and C_{44} at a very small volumetric content of a fluid with a subsequent increase in the elasticity moduli as the sample completely dries is a distinction of kind as compared to other known dependences.

4.1. Estimations of Elasticity Moduli Variations Attributed to Capillary Forces

An increase in the elasticity moduli during sandstone drying in [11] is explained by compression of grains caused by capillary forces in the region of the grain contact. This assumption was not confirmed by any estimates, as is the case with other works (see review [12] and later work [21]). The lack of a quantitative analysis of the data in [11, 12, 21] is likely to be attributed to the absence of the data of an independent granulometric analysis in these works. A complex character of the investigations in our study allows for checking the validity of the earlier-made explanation within the framework of elementary models of granulated media. The volumetric ($K = C_{11} - 4C_{44}/3$) and shear ($G \equiv C_{44}$) stiffness of packing of the balls pressed to one another by the uniform pressure is determined by the expressions [16]

$$K_{\text{eff}} = \frac{C(1-\phi)}{12\pi R} S_n, \quad G_{\text{eff}} = \frac{C(1-\phi)}{20\pi R}(S_n + 3S_\tau/2),$$

where ϕ is the porosity, R is the radius of spherical grains, C is the coordination number (the average number of contacts for each sphere), and S_n and S_τ are the compression and shear stiffness of each pair of contacting grains (see also [22]):

$$S_n = \frac{4Ga}{1-\nu}, \quad S_\tau = \frac{8Ga}{2-\nu},$$

where $G = E/2(1+\nu)$ is the shear modulus of the grain material (or its effective value during a contact of grains from different materials (see [22]), a is the radius of the point contact patch ($a \ll R$). The approach of the sphere centers h and the radius of the contact patch a are

$$h = a^2/R, \quad a^3 = \frac{3FR}{4E^*},$$

where F is the force compressing the spheres and E^* is the equivalent stiffness modulus (see [15, 22]): $(E^*)^{-1} = (1-\nu_1^2)E_1^{-1} + (1-\nu_2^2)E_2^{-1}$.

Since S_n and S_τ depend on the radius of the contact patch in a similar way an increase in the compression pressure in to be accompanied by similar relative increases in the shear moduli $G_{\text{eff}} \equiv C_{44}$ and volumetric stiffness $K_{\text{eff}} \equiv C_{11} - 4C_{44}/3$. The data (a dashed line in Fig. 5) correspond to the variations in $\Delta G_{\text{eff}} \simeq 0.7$ GPa and $\Delta K_{\text{eff}} \simeq 0.7$ GPa with an increase in saturation from 1 to 10%. The values $K_{\text{eff}} \simeq 19.5$ and $G_{\text{eff}} \simeq 18$ GPa for $S = 10\%$ practically coincide and, thus, relative moduli variations are nearly equal. Thus, the mechanism responsible for an increase in the elasticity moduli with a decrease in saturation can be soundly attributed to variations in the grain compression pressure.

The following model can be proposed to explain the dependences of Fig. 5. Stage 1 can be determined as a stage of moisture condensation on the pore walls and formation of a monomolecular layer of a fluid that yields a decrease of the cohesion force with an increase in S. Stage 2 is related with the formation of menisci at the places of grain contacts and formation of capillary forces of grain compression. Finally, stage 3 can be determined as a stage of gradual filling of the entire pore space with a fluid that yields a decrease in the contribution of capillary forces.

Let us estimate the pressure that corresponds to capillary compression of grains and ascertain that the proposed model is reasonable. First, let us estimate the strain sensitivity of limestone. For this, let us make use of the thermodynamic relationship [23] and express the value of interest through volume derivatives:

$$\left.\frac{\partial K}{\partial P}\right|_{P=0} = -V_0 \frac{\partial^3 \mathscr{E}}{\partial V^3} \Big/ \frac{\partial^2 \mathscr{E}}{\partial V^2} = \frac{-6\mathbb{C}}{K_0 - 2G_0/3},$$

where $\mathscr{E}$ is the free Helmholtz energy, $\mathbb{C}$ is the Landau modulus [15], K_0 and G_0 are the moduli of volumetric stiffness and shear at a zero pressure, $K_0 \simeq 20$ GPa and $G_0 \simeq 18$ GPa. Let us specify the Landau modulus based on the data of [24], where the Landau moduli of the rock, including limestone with similar porosities and densities, were measured (also see Table 1, which shows that the parameters of the analyzed sample are typical for limestone): $\mathbb{C} \sim -2000$ GPa. Thus, we get the following estimate of the strain sensitivity:

$$\frac{\partial K}{\partial P} \sim 10^3. \tag{1}$$

This equation makes it possible to estimate the pressure that is to be created inside the limestone to increase the modulus of the volumetric stiffness by 0.7 GPa. It can be easily seen that for the observed variations to be explained it is necessary to assume that the pressure inside the sample in $P \sim 0.7$ MPa.

The capillary pressure is described by the following equation [16]:

$$P_c = \gamma\left(\frac{1}{R_1} - \frac{1}{R_2}\right)\cos\theta,$$

where $R_1 = R(\sin\varphi + \cos\varphi - 1)/\cos\varphi$, $R_2 = R(1-\cos\varphi)/\cos\varphi$, γ is the coefficient of surface tension, θ is the contact angle (which is assumed hereinafter to be zero), $R_{1,2}$ are the curvature radii, R is the grain radius, and φ is the angle between the line connecting the centers of contacting grains and that from the grain center to the point on the boundary of the wetted surface, For small angles $\varphi \ll 1$ $P_c \simeq -\frac{2\gamma}{R\varphi}$, where the minus sign corresponds to the grain compression. The volume occupied by the meniscus between each grain pair is $V_f \simeq 0.793\pi R^3\varphi^4$, $\varphi \ll 1$.

Let us carry out elementary estimations. The maximal variations in the elasticity moduli are observed at $S \simeq 0.5\%$ and correspond to the total volume of the

capillary fluid inside the sample $\Sigma V_f = NV_f \simeq 135$ mm^3, where $N = \mathcal{N}\mathcal{C}$ is the total number of contacts equal to the product of the number of grains and the (coordination) number of contacts for each grain. Assuming the fluid to be uniformly distributed inside the sample, let us estimate the number of grains as a ratio of the sample volume $V_0 \simeq 1.5 \times 10^5$ mm^3 and the grain volume $\mathcal{N} \sim \dfrac{V_0}{4\pi R^3/3}$. For the porosity $\phi = 18\%$ in case of a random packing of grains the coordination number is $\mathcal{C} \simeq 15$ [16]. Thus, $N \approx \dfrac{\mathcal{C}V_0}{4\pi R^3/3}$ and, as a result, the characteristic volume of the meniscus is

$$V_f \approx \Sigma V_f \frac{4\pi R^3}{3\mathcal{C}V_0} = 0.793\pi R^3 \varphi^4.$$

It can be easily seen that the angle φ does not depend on the grain size R and is

$$\varphi \approx \left[\frac{1.68\Sigma V_f}{\mathcal{C}V_0}\right]^{1/4} \approx 0.1 = 5.7^\circ. \quad (2)$$

For this angle (2), the required compression pressure of 0.7 MPa is obtained for the characteristic grain size (the surface tension coefficient of water is $\gamma = 0.075$ N/m), which is $R \lesssim 2$ μm. It is apparent from Fig. 3 that the analyzed sample contained a sufficient number of grains with such sizes. Thus, the observed variations in the elasticity moduli at stages 2 and 3 can be soundly related to the existence of capillary forces during menisci formation.

4.2. Comparison with the Data of Other Studies

The authors of [18] demonstrate the data obtained for different natural materials during pore filling with a fluid. On average, a variation in the shear wave velocity is about 5%, which corresponds to a 10% variation in the shear modulus. In the present paper, relative variations in shear and volumetric stiffness are also approximately 10%. Thus, we have quantitative agreement with the known experimental results.

As follows from the data of [24], the Massilon sandstone analyzed in [11] is characterized by practically the same strain sensitivities as the limestone considered by us. A twofold increase in velocities corresponds to a fourfold increase in the elasticity moduli. Studies [11] make it possible to estimate the volumetric and shear stiffness as $K \simeq 1.6$ and $G \simeq 1.7$ GPa, i.e., nearly one order lower as compared to the stiffness of the limestone analyzed by us. Note that a negative Poisson coefficient corresponds to these values. It is interesting to note that the author of [11] gives the data either for wave velocities or their ratios, paying no interest in the value of the Poisson coefficient ν. There are model considerations concerning $\nu < 0$ in heterogeneous media (see, e.g., [25]). Nevertheless, the negative value of the Poisson coefficient for the data [11] points, in our opinion, to incorrect comparison of the data obtained using the method of the longitudinal and torsional pendulum in different samples. Note that according to our data the Poisson coefficient is $\nu = 0.12$ for a dry sample and $\nu = 0.15$ for a completely saturated one.

A fourfold stiffness increase corresponds to the capillary pressures of about 2 MPa that corresponds to the curvature radius of contacting grain surfaces $R \lesssim 1$ μm. The average size of sandstone grains was 150–200 μm (see Table 1 in [11]) that is two orders larger than R. It seems that velocity variations at the moisture content less than 1% observed in [11] can be explained by formation of menisci at irregularities of the contacting grains. Recall that the results of the granulometric analysis of the samples are absent in [11].

It can be assumed that sharp qualitative changes taking place inside limestone should be accompanied by substantial variations in nonlinear acoustic characteristics. One should pay attention to [21], the authors of which observed a one-order increase in the hysteresis nonlinearity parameter at saturation changes from 0.1 to 30%, i.e., in the saturation range where a transition from stage 1 to stage 2 takes place (Fig. 5). The authors of [21] proposed a model of the moisture effect on the acoustic properties that was analogous to ours but did not verify their hypothesis by any estimates and did not reveal the S-shaped dependence of the elasticity moduli we recorded (Fig. 5). The authors of [21] related the reasons for the appearance of the hysteresis in a carbonate rock, which was anomalous as compared to that in sandstone to a complex structure of hollows with the characteristic sizes up to 1 nm. Based on the absorption-desorption curves the capillary pressure was estimated in [21] as $\sim 10^8$ Pa, which corresponds to particles about 20 nm in size. On the other hand, changes in the Young modulus at the limestone saturation came to $\simeq 3\%$, which agrees in order of magnitude with our data. The revealed slight variations in the Young modulus seem to be related to a low concentration of particles with 20-nm sizes. The results of the granulometric analysis in [21] are absent.

It is interesting to note that we observed inflections in the measured dependences for both the elasticity moduli and the loss coefficients at one and the same saturation values. These peculiarities are seen in Fig. 5 at $S = 0.1$, 0.8, and 8–20% and are likely to be related to qualitative variations in the character of fluid distribution inside limestone. In particular, using elementary calculations one can get convinced that the value $S \approx 10\%$ corresponds to closing of the menisci between four spheres with similar sizes that form a pyramid. The saturating increasing further, the pore space is gradually filled with a fluid. Thus, starting from $S \sim 10\%$, we can speak about a macroscopic motion of the

fluid with respect to the skeleton that is accompanied by a smooth increase in attenuation in Fig. 5.

4.3. Estimated Limestone Permeability. Mechanisms Responsible for Attenuation of Acoustic Waves

The analysis of dispersion dependences was aimed at revealing characteristic frequencies associated with relative displacements of the fluid and the skeleton as well as determination of frequency dependences of loss coefficients. The Bio frequency, which is responsible for transition to the mode of a slow Bio wave propagation (the equality of viscous and inertial forces), is [16]:

$$f_c = \frac{\phi\eta_f}{2\pi\rho_f\kappa}, \quad (3)$$

where η_f is the dynamic viscosity of a fluid, ρ_f is the fluid density, and κ is the absolute permeability of a porous body.

It is impossible to exactly calculate permeability for a porous medium with an arbitrary microstructure. Most analytical results refer to ordered media and the media whose porosity is large, namely $\phi \sim 1$. In the region where the porosity ϕ is close to the threshold of percolation ϕ_c, the permeability value strongly depends on the material microstructure, which is often unknown. Nevertheless, the percolation threshold is well approximated by the equation [26]

$$\phi_c = \frac{D}{\mathcal{C}(D-1)},$$

where D is the system dimensionality (in our case, $D = 3$) and $\mathcal{C}$ is the coordination number (in our case, $\mathcal{C} = 15$). The value of $\phi_c = 10\%$ is two times lower than the measured porosity of the sample $\phi = 18\%$, which points to the presence of a system of bound pores.

The permeability will be estimated using the empirical Kozeni–Carman formula [17], with the correction for the percolation threshold being taken into account (also see [16]):

$$\kappa = \frac{d^2(\phi-\phi_c)^3}{180(1-(\phi-\phi_c))^2}, \quad (4)$$

where d is the characteristic diameter of granule grains. Here, $d = 0.2$ mm (Fig. 3) and the estimate is $\kappa \simeq 1.2\times10^{-13}$ m^2 or 123 mD. To check the formula we use the data of [11]. The measured permeability was 737 mD, and its estimation using the formula (4) gives $\kappa \simeq 966$ mD, which agrees in order of magnitude with the data of the direct measurements. The permeability value makes it possible to estimate the characteristic size of the pores corresponding to the bound porosity. For the Poiseuille flow [27], the value is $\kappa = d_c^2/2$, where d_c is the diameter of the capillary tube. The size of the bound pores in the analyzed limestone sample can be estimated as $d_c = \sqrt{2\kappa} \sim 0.5$ μm.

The characteristic frequency (the frequency of the absorption maximum) estimated using the formula (3) is $f_c \sim 240$ kHz, which is substantially higher than the frequencies at which the acoustic measurements were performed. Thus, wave motions of the fluid in capillaries were absent and the acoustic measurements (Section 2) were performed for viscous fluid flow antiphase to the oscillations of the skeleton [28]. The time of diffusion (relaxation) of pressure in the pores in the acoustic wave field is $\tau \approx L^2/\mathcal{D}$, where L is the characteristic spatial scale, $\mathcal{D} = \kappa K_f/\eta_f\phi$ is the diffusion coefficient, and K_f is the volumetric stiffness of the fluid [29]. The equation that described relaxation of pressure perturbations in the pores has the form [29]

$$\frac{\partial p}{\partial t} - \mathcal{D}\nabla^2 p = 0, \quad (5)$$

where it is implicitly assumed that the diffusion coefficient $\mathcal{D}$ is the same in the entire porous body.

Let us estimate the characteristic spatial scales. The equation (5) makes it possible to determine a relationship between the depth of the perturbation penetration and the frequency, $\delta_D = \sqrt{2\mathcal{D}/\omega}$. For the analyzed limestone, the diffusion coefficient is $\mathcal{D} \simeq 1.5$ m^2/s. In the frequency range of 10–40 kHz $\delta_D = 3$–7 mm. This scale is slightly smaller than the sample size that excludes the appearance of corresponding absorption maxima (see Figs. 5, 7). The thickness of the fluid skin-layer is $\delta_v = \sqrt{2\nu_f/\omega}$, where ν_f is the kinematic viscosity ($\nu_f = 10^{-6}$ m^2/s for the water with the temperature 20°C), and ω is the circular frequency [27].

In the frequency range of 10–40 kHz the skin-layer thickness is $\delta_v = 3$–6 μm, which substantially exceeds the characteristic size of the bound pores d_c.

Note that the absorption maximum observed in [11] seems not to be related to the mechanism of fluid extrusion from the intergrain space as the author assumed, but is explained by flowing of the fluid across the sample. Really, the absorption maximum was observed in [11] at the frequencies of 3–4 kHz, which correspond to the scale $\delta_D \approx 2.4$ cm at the transverse dimensions of the sample equal to 2.2 cm. Thus, the absorption maximum corresponds to the "resonance" of a slow (diffusion) Bio wave. As it is expected, the absorption maximum shifted to the high-frequency region with a decrease in the saturation degree (a decrease in characteristic dimensions of the regions filled with a fluid).

The absence of the frequency dependence η_{ij} means invariability of attenuation at a distance equal to the wavelength. On the other hand, within the framework of the Bio theory [28], the values of η_{ij} in the region of low frequencies when the inequality $d_c < \delta_v$ is valid will linearly increase with an increase in

frequency. The absence of the frequency dependence of the attenuation coefficient (Fig. 7) during changes of absorption from 0 to 90% which is characteristic for the Bio theory [28] motivates to consider the problem of the mechanism of acoustic losses in porous materials during saturation with a fluid in greater detail.

First of all, it is necessary to note that there are a variety of opinions in the literature concerning the frequency dependence of the loss factor in porous materials and, in particular, in sedimentary rock. For example, in review [30] and other works, the author, based on the analysis of a large body of data, draws a conclusion on the absence of the frequency dependence of the loss factor and sound velocity dispersion. In [31] this point of view is called in question and the author gives the experimental data which are in agreement with the Bio theory. In the brief communication [32] a possible additional energy outflow to a near-bottom waveguide is considered as a possible reason of a disagreement between the experiment and the theory. The author of [33] remarks that a modern level of measurements made it possible to reveal a weak logarithmic dispersion of the sound velocity in sedimentary rock, which is characteristic for $\eta_{ij} \propto \omega_0$ [16]. The same work gives a comparison of the experimental data with different theoretical models and shows a good agreement with the model of [34] based on the assumption of nonlinear microscopic flows in the region of contact of rough grains. Thus, the analysis of the literary data points to the absence of a unified point of view on the mechanisms of attenuation and the frequency dependence of lass factors in sedimentary rock.

The data shown in Figs. 5 and 7 make it possible to propose elementary model considerations as a current hypothesis for explaining attenuation mechanisms. Let us make simple estimations based on geometrical considerations. About 60–70% of limestone consist of the grains with the size $D \approx 0.2$ mm (Fig. 3). The size of the hollows inside a dense packing of identical spheres is estimated as $D_v = 0.15D \approx 30$ μm [16]. Based on the results of petrographic investigations the pore length varies within a wide range and is $L_p = 50–10^4$ μm. The ratio of pore and hollow volumes can be estimated as $(\pi D_v^3/6)$, $(\pi d_c^2/4) \sim 10–10^3$, which corresponds to variations in the degree of saturation within the range of 0.1–10%. Thus, there is a minor concentration of a fluid in bound pores.

In case of complete saturation, the attenuation is determined by the fluid motion in the pores and filled hollows. Since the hollows occupy a larger volume and their sizes exceed the penetration depth δ_v, the values of η_{ij} should have a root dependence of frequency [27]. The frequency dependence of $\eta_{44} \propto \omega^{0.4}$ (Fig. 7, insert) corresponds to the minimal root-mean-square error. However, the dependence of $\eta_{44} \propto \omega^{1/2}$ also is in a satisfactory agreement with the experimental data, the confidence intervals being taken into account. As for the absorption characteristics by the longitudinal wave η_{11}, the accuracy of measuring this parameter unfortunately turned out to be insufficient for determining its frequency dependence.

On the other hand, some hollows during sample drying turn out to be unfilled and menisci are formed. Their deformation is accompanied by the processes of absorption and desorption a capillary hysteresis (delay) complies with that should be accompanied by absorption of the oscillation energy. It can be assumed that there is are large number of space–time scales corresponding to relaxation processes. In this case, as is seen from the results of [35], the loss coefficients weakly depend on frequency, $\eta_{ij} \propto \omega^0$.

A transition from the absorption mode with $\eta_{44} \propto \omega^{1/2}$ to the mode with $\eta_{44} \propto \omega_0$ takes place at $S \lesssim 95\%$ that points to a relative volume occupied by thin pores which is not more than 5%. This value agrees well with the "geometric" estimation given above. Thus, the proposed hypothesis seems reasonable. It is in agreement with the obtained experimental data and can be used to explain deviations in the interpretation of the literary data on attenuation in bottom sedimentary rock.

5. CONCLUSIONS

All three stages in the process of saturation of a granulated porous body with a fluid, namely, moisture condensation, formation of menisci, and gradual filling of hollows and pores, were distinguished using the method of acoustic spectroscopy. The characteristics of both longitudinal and shear waves were analyzed in the 2-octave range.

In addition, the data were obtained for one and the same sample for which variations in the elasticity moduli being in agreement with the experimental data were estimated. These two peculiarities distinguish the present study from those published earlier [11, 12], where all saturation stages were not simultaneously observed and the mechanisms responsible for the observed changes of the measured quantities were not analyzed.

It is shown that a fluid substantially changes the skeleton properties that should be taken into account when construction the models of sound propagation in granulated porous media. Attenuation of longitudinal and shear waves depends on the presence of a fluid even when the saturation degree is about 0.1%. The analysis of the frequency dependence of attenuation made it possible to make reasonable assumptions on the attenuation mechanisms and on the character of hollow and pore filling, which agree with elementary geometric considerations. The revealed nature of variations in the frequency dependence during transition from partial to complete saturation seems to be related to the explanation of the existing divergences during interpretation of acoustic wave attenuation in the

ocean, which is attributed to energy absorption in water-saturated sedimentary rock.

ACKNOWLEDGMENTS

The study was supported in part by the Russian Foundation for Basic Research (projects nos. 08-02-00670 and 08-05-97014) and the Russian Academy of Sciences program "Coherent Acoustic Fields and Signals."

REFERENCES

1. A. Migliori and J. L. Sarrao, *Resonant Ultrasound Spectroscopy* (Wiley, 1997).
2. N. Lucet and B. Zinszner, Geophysics **57**, 1018 (1992).
3. V. S. Averbakh, V. V. Artelnyy, B. N. Bogolyubov, V. V. Bredikhin, A. V. Lebedev, A. P. Maryshev, and V. I. Talanov, Akust. Zh. **54**, 84 (2008) [Acoust. Phys. **54**, 71 (2008)].
4. A. V. Lebedev, V. V. Bredikhin, I. A. Soustova, A. M. Sutin, and K. Kusunose, J. Geophys. Res. **108** (B10), EPM11 (2003).
5. M. Mah and D. R. Schmitt, Geophysics **66**, 1217 (2001).
6. Z. Wang, Geophysics **67**, 1415 (2002).
7. E. P. Papadakis, J. Acoust. Soc. Am. **45**, 1547 (1969).
8. H. J. McSkimin, J. Acoust. Soc. Am. **33**, 12 (1961).
9. G. A. Gist, J. Acoust. Soc. Am. **96**, 1158 (1994).
10. J. E. White, *Seismic Waves: Radiation, Transmission and Attenuation* (McGraw-Hill, New York, 1965; Nedra, Moscow, 1986).
11. W. F. Murphy, J. Acoust. Soc. Am. **71**, 1458 (1982).
12. K. W. Winkler and W. F. Murphy, in *A Handbook of Physical Constants*, Ed. by T. J. Ahrens, Vol. 3 (Amer. Geophys. Union, Washington, DC, 1995), pp. 20–34.
13. A. V. Lebedev, V. V. Bredikhin, and I. A. Soustova, in *Proc. of the Seminar of Prof. S.A. Rybak Sci. School* (Russ. Acoust. Soc., Moscow, 2003), pp. 77–92.
14. A. V. Lebedev, Akust. Zh. **48**, 381 (2002) [Acoust. Phys. **48**, 339 (2002)].
15. L. D. Landau and E. M. Lifshitz, *Course of Theoretical Physics*, Vol. 7: *Theory of Elasticity* (Nauka, Moscow, 1982; Pergamon Press, New York, 1986).
16. G. Mavko, T. Mukeji, and J. Dvorkin, *The Rock Physics Handbook. Tools For Seismic Analysis in Porous Media* (Cambridge Univ., Cambridge, MA, 1998).
17. J. G. Berryman, in *A Handbook of Physical Constants*, Ed. by T. J. Ahrens, Vol. 3 (Amer. Geophys. Union, Washington DC, 1995), pp. 205–228.
18. J. Khazanehdari and J. Sothcottz, Geophysics **62**, 472 (2003).
19. A. N. Tutuncu and M. M. Sharma, Geophysics **57**, 1571 (1992).
20. F. D. Shield, M. Sabatier, and M. Wang, J. Acoust. Soc. Am. **108**, 1998 (2000).
21. K. E.-A. Van Den Abeele, J. Geophys. Res. **107** (B6), 101029 (2002).
22. K. Johnson, *Contact Mechanics* (Cambridge Univ., Cambridge, 1985; Mir, Moscow, 1989).
23. I. P. Bazarov, *Thermodynamics, The Schoolbook* (Vysshaya shkola, Moscow, 1991) [in Russian].
24. K. W. Winkler and Liu. Xingzhou, J. Acoust. Soc. Am. **100**, 1392 (1996).
25. V. Yu. Zaĭtsev and P. Sas, Fiz. Mezomekh. **7**, 37 (2004).
26. M. Sahimi, *Heterogeneous Materials: Morphology, and Linear Transport and Optical Properties. Volume 23. Interdisciplinary Applied Mathematics* (Springer, New York, 2003).
27. L. D. Landau and E. M. Lifshitz, *Course of Theoretical Physics*, Vol. 2: *The Classical Theory of Fields* (Nauka, Moscow, 1988; Pergamon, Oxford, 1975).
28. M. A. Biot, J. Acoust. Soc. Am. **28**, 168 (1956).
29. R. Chandler, J. Acoust. Soc. Am. **70**, 116 (1981).
30. E. L. Hamilton, J. Acoust. Soc. Am. **59**, 528 (1976).
31. R. D. Stoll, J. Acoust. Soc. Am. **77**, 1789 (1985).
32. W. M. Carey, A. D. Pierce, R. E. Evans, and J. D. Holmes, J. Acoust. Soc. Am. **124**, EL271 (2008).
33. M. J. Buckingham, J. Acoust. Soc. Am. **117**, 137 (2005).
34. M. J. Buckingham, J. Acoust. Soc. Am. **108**, 2796 (2000).
35. B. Hartmann, G. F. Lee, and J. D. Lee, J. Acoust. Soc. Am. **95**, 226 (1994).
36. J. D. Bass, in *A Handbook of Physical Constants*, Ed. by T. J. Ahrens, Vol. 2 (Amer. Geophys. Union, Washington DC, 1995), pp. 45–63.